Authors' accepted manuscript
Article published in ACS Applied Materials and Interfaces, Vol. 13, no 37, 2023, pp.44673-44685.
The final published version available at https://dx.doi.org/10.1021/acsami.1c07540

Efficient and recyclable heterogeneous catalyst based on PdNPs stabilized on green-synthesized graphene-like nanomaterial: effect of surface functionalization

Samia Mahouche-Chergui[1,], Abdallah Oun[1], Imane Haddadou[2], Clémentine Hoyez[1], Laurent Michely[1], Claudiane Ouellet-Plamondon[2], Benjamin Carbonnier[1]*

[1] Univ Paris Est Creteil, CNRS, ICMPE, UMR 7182, 2 rue Henri Dunant, 94320 Thiais, France

[2] École de Technologie Supérieure, University of Québec, Montréal, QC, Canada

*Corresponding author: mahouche-chergui@icmpe.cnrs.fr
Laboratory ICMPE, University of Paris-Est Créteil, 2-8, rue Henri Dunant, 94320, Thiais, France

ABSTRACT:
A straightforward and efficient approach was reported to surface functionalize graphene-like nanomaterial with abundant carboxylic acid groups for anchoring palladium nanoparticles with a highly increased stability and their use as highly active and stable heterogeneous catalyst for the reduction of both cationic (methylene blue, MB) and anionic (eosin-Y, Eo-Y) toxic organic dyes. The large specific surface area (S_{BET} = 266.94 m^2/g) graphene-like nanomaterial (GHN) was prepared through green and cost-effective pyrolysis process from saccharose using layered bentonite clay as a template. To introduce a high density of carboxylic acid functions, GHN nanomaterial was first doubly functionalized by successive grafting of (3-glycidyloxypropyl)trimethoxysilane (GPTMS) and tris(4-hydroxyphenyl)methane triglycidyl ether (TGE) using two different approaches. The GHN nanomaterial functionalized with more epoxide functions was then selected for further functionalization with carboxylic acid functions via a ring-opening reaction through a two-step hydrolysis (H_2SO_4)/oxidation ($KMnO_4$) approach. The GHN nanomaterial bearing carboxylic acid groups was then treated with sodium hydroxide to produce deprotonated carboxylic acid-rich support. Finally, GHN-COO^- binds strongly a high density of Pd^{2+} ions to form stable complexes which after reduction by $NaBH_4$ leads to highly dispersed, densely anchored and uniformly distributed PdNPs on the surface of the functionalized GHN. The obtained GHN-COO@PdNPs nanohybrid revealed an excellent catalytic activity in the reduction of MB and Eo-Y by an excess of $NaBH_4$ at room temperature with pseudo first-order rate constant (k_{app}) values of 1.65 x 10^{-2} and 0.93 x 10^{-2} s^{-1}, respectively. In addition, the obtained results indicated that the as-synthesized catalyst exhibited excellent recyclability showing more than 94% conversion of MB dye even after eight consecutive runs. The high catalytic performance can be attributed to the high dispersion, stability, and no leaching of the GHN-supported PdNPs, which undoubtedly resulted from the efficiency of the GHN surface functionalization. Moreover, the high reactivity of the epoxy groups grafted onto GHN makes it versatile sustainable platform for the formation and stabilization of metallic nanoparticles of different nature leading to promising heterogeneous nanocatalysts for a broad range of catalytic reactions.

Keywords: sustainable graphene-like nanomaterial, epoxy-surface modifiers, palladium nanoparticles, heterogeneous catalysis, organic dyes removal.

Authors' accepted manuscript
Article published in ACS Applied Materials and Interfaces, Vol. 13, no 37, 2023, pp.44673-44685.
The final published version available at https://dx.doi.org/10.1021/acsami.1c07540

1. INTRODUCTION

Decoration of solid supports with nano-sized metallic nanoparticles is of great interest in tuning materials properties for the fabrication of advanced hybrid materials for varied applications ranging from electronics,[1] life sciences,[2] energy storage,[3] and sensing,[4] to heterogeneous catalysis.[5]

Nano-sized metallic particles possess unique optic and electronic properties.[6] In addition to these properties, they have a remarkable surface-to-volume ratio, resulting in a high number of available active sites per unit area in comparison with their bulk analogs, making them excellent candidates for catalysis.[7] However, this feature is often strongly altered, when the metallic nanoparticles (MNPs) are used alone, they tend to agglomerate because of their high surface free energy. This induces a strong decrease in their thermodynamic dispersion stability and hence the loss of their surface area resulting in a drastic decrease in MNPs properties such as catalytic activity. Indeed, it is known that the catalytic performances of MNPs is intimately related to their size and stability.[8] To improve the MNPs dispersion and to take full advantage of the benefits of nanosized effect, it is necessary to support the metallic nanoparticles by a solid platform such as polymers,[9] clay nanoparticles,[10] mesoporous silica,[11] cellulose nanoparticles,[12] carbon nanotubes,[13] and graphene nanoplatelets,[14] to name but a few. In particular, graphene, as a 2D monolayer of graphite, has been emerging as a promising supporting material for MNPs due to its several unique properties, such as ultrasmall dimension, extraordinary specific surface area, unique mechanical, thermal, chemical, optical and electrical properties, as well as excellent electron transport property at room temperature.[15] Graphene-based nanostructures have also shown great potential in heterogeneous catalysis. [16-17]

However, despite these remarkable properties there are critical limitations to the practical applications of pristine graphene-supported MNPs in heterogeneous catalysis related to, on the one hand, the aggregation of graphene nanoparticles due to the strong π- π stacking interactions between graphene nanolayers, and on the other hand, the weak interactions between graphene and MNPs which result in a poor control of the size and the dispersion stability of the MNPs, thereby making the catalytic active sites inaccessible.[18] Chemical surface modification of graphene with suitable functional entities exhibiting high binding affinity to metal ions can be used for the direct generation of metal nanoparticles having finely controlled size, morphology, size distribution, and density on the surface of the support. This is a powerful strategy for designing highly stabilized and homogeneously dispersed MNPs.[19] The functionalization is very versatile as it enables the introduction of various desired functional moieties including

amine, thiol, phosphonic, sulphonic and carboxylic acid, and so on, providing an opportunity for in-situ designing a wide variety of catalytic systems by using reducing agents like hydrazine, ascorbic acid, sodium citrate, sodium borohydride.[20-21] Furthermore, graphene surface functionalization has a dual role, namely, improving ability to anchor and stabilizing MNPs, and enhancing the dispersion of graphene, because the functional surface modifiers act also as surface passivation agents. Although functionalized graphene/MNPs systems exhibit interesting catalytic properties, their stability is compromised by the stability of the interface between graphene support and the functional groups.[22] To date, strategies including non-covalent and covalent chemical modification methods have been developed to design MNPs-decorated graphene nanohybrids.[23] The covalent surface functionalization strategy is expected to be more appropriate as it provides much stronger interfacial adhesion compared to that obtained with the non-covalent one. This leads to more stable and highly resistant hybrid nanocatalysts preventing metal leaching. Furthermore, the stability of nanocatalysts plays a key role not only because it preserves a desirable catalytic activity during recyclability/reusability tests but also it prevents toxic effect of leached metal nanoparticles that are difficult to recover from solution.[24] Palladium nanoparticles (PdNPs) are one of the most commonly used transition metal nanoparticles as green catalysts for the efficient synthesis of chemical intermediates utilized in the design of pharmaceutical and agricultural chemicals, antioxidants, pigments for advanced materials using, for example, cross-coupling [25], or annulation oxidative reactions.[26] In addition, PdNPs in the presence of hydrogen donors have been applied as efficient catalysts in the selective conversion of toxic compounds such as dyes into environmentally benign ones through the cost-effective and environment-friendly hydrogenation reactions [27-28].

Indeed, the high aqueous solubility of dyes and their wide use in several industrial fields such as pharmaceutical,[29] food,[30] paint,[31] paper,[32] and textile,[33] lead to their inevitable presence in wastewater which can have significant impact on environment and human health because of their acute toxicity.

With the same aim of respecting the environment, nowadays, development of a new generation of renewable and cost-effective value-added chemicals such as catalysts from sustainable, widely available, and low-cost precursors through environmentally friendly procedures is crucial. For this, graphene-clay nanomaterial was initially synthesized *via* a green pyrolysis process from saccharose, a natural disaccharide used as a carbon source, and bentonite, a natural inorganic multilayered nanomaterial acting as nanostructured template for graphene layers formation. The as-synthesized graphene-like nanomaterial (GHN) was then

successfully functionalized by epoxy reactive moieties, involving for the first time alkoxysilane surface modifier coupled with tris(4-hydroxyphenyl)methane triglycidyl ether (TGE). Alkoxysilanes are known to be powerful molecules for covalent modification of hydroxyl-containing surfaces while tris(4-hydroxyphenyl)methane triglycidyl ether has shown its efficient grafting on carbonaceous materials.[34-35] TGE trifunctional epoxy was used here as a surface modifier for covalent functionalization of graphene sheets in GHN, following a method previously reported by Martinez-Rubi for producing a soft covalently bonded interface around SWCNT.[36]

The objective of such functionalization is to incorporate a high amount of tightly anchored epoxy-rich molecules onto the surface of GHN allowing to improve its dispersibility and at the same time to confer it strong chelation properties, enabling immobilization of a large number of small-sized palladium particles with uniform size and dispersion. For this, two different strategies were compared; on the one hand, GHN was first silanized with (3-glycidyloxypropyl) trimethoxysilane (GPTMS) and then bifunctionalized by chemical grafting of TGE. On the other hand, silanization of GHN using GPTMS was conducted after grafting of TGE. Then, GHN-GPTMS-TGE, the doubly functionalized nanomaterial with the largest number of epoxy moieties was treated with H_2SO_4/ $KMnO_4$ to ring-opening of the attached reactive epoxy groups to convert them to chelating carboxylic acid groups,[37] which after deprotonation have been exploited to anchor a large number of Pd^{2+} metallic ions via complexation reaction. The complexed Pd^{2+} ions were subsequently in-situ reduced for the generation of uniformly dispersed nano-scale palladium particles on GHN surface. Finally, the newly designed GHN-COO@PdNPs nanohybrid material was used as efficient and recyclable heterogeneous nanocatalyst in reduction of different types of dyes.

2. EXPERIMENTAL SECTION

2.1. Materials. The sodium bentonite clay (BT) was purchased from Canadian Clay Products, Inc (65-85 meq/100g ion-exchange capacity, 2.6 g/cm^3 density) and used without further treatment. All the following chemicals were purchased from Sigma-Aldrich and used as received: saccharose ($C_{12}H_{22}O_{11}$, 99.5 %), (3-glycidyloxypropyl)trimethoxysilane (GPTMS, $C_9H_{20}O_5Si$), tris(4-hydroxyphenyl)methane triglycidyl ether (TGE, $C_{28}H_{28}O_6$), sodium cubes, contains mineral oil, 99.9% trace metals basis), naphthalene (99%), palladium chloride

(≥99.9%), anhydrous toluene (99.8%), anhydrous tetrahydrofuran (99.8%) and sodium borohydride ($NaBH_4$, 99%). The 0.1N sodium hydroxide (NaOH) was purchased from VWR Chemicals BDH Prolabo. The aqueous solutions used in this work were prepared with Millipore water (DI water).

2.2. Synthesis of GHN. Graphene-like hybrid nanomaterial was prepared according to the previously described eco-friendly method where natural clay and saccharose were used as precursor materials [38]. Firstly, homogenized BT particles (<2µm) were vigorously dispersed in DI water at 83.3 % by weight. After 24 h of swelling at room temperature, the resulting suspension was mixed for 20 min with an aqueous solution of saccharose (2 g/mL) in 1:5 weight ratio (BT: saccharose) using a Velp mixer with a stirring speed of 400 rpm. Subsequently, the mixture was dried in an oven for 48 h at 50°C, followed by an activation in a furnace at 750°C for 1 h under nitrogen flow. Finally, the obtained dark monolith was ground using a mortar and pestle (Pulvirisette 6, Laval Lab Inc.) until the particle size is less than 20 µm.

2.3. GPTMS surface functionalization of GHN (GHN-GPTMS). Initially, 100 mg of GHN powder was homogeneously dispersed in 50 ml of 0.1M HCl under stirring for 15 min. The mixture was then ultrasonicated for 30 min to separate the sheets between them and facilitate the clay surface protonation. The suspension was filtered and rinsed with distilled water several times to remove Cl^- and any impurities, followed by a drying step at 60°C under vacuum. The activated graphene/clay GHN-OH was recovered for further use. GHN-GPTMS was prepared by dispersing 100 mg of GHN-OH in 50 ml of anhydrous toluene followed by adding of 5 mmol of GPTMS under magnetic stirring. The reaction mixture was heated at 50 °C and the suspension was kept under stirring for 16 h under an inert atmosphere. The silanized product was collected by centrifugation after vigorous washing with water and ethanol and later dried at 60 °C overnight.

2.4. TGE surface functionalization of GHN (GHN-TGE). Prior to TGE grafting on the surface of GHN and in order to improve its dispersion, GHN was treated with an alkali metal (Na) in the presence of naphthalene which plays the role of electron transfer mediator.[39] Then, 100 mg of GHN was dispersed in 50 ml of anhydrous toluene by stirring for 15 min and sonication for 30 min. Separately 550 mg of naphthalene and 100 mg of sodium were mixed in

100 mL of anhydrous toluene with constant stirring at room temperature for few minutes. The colloid solutions were mixed under an inert atmosphere for 16 h of stirring. Afterwards, the reaction mixture was washed by ethanol dropwise addition till the disappearance of the observed gas release, indicating the complete removal of unreacted sodium. The reaction mixture was subsequently purified through successive rinsing steps with ethanol, water and then with acetone. Then it was dispersed in 100 mL of anhydrous THF by magnetic stirring and ultrasonication for 15 min, 5 mmol of TGE was added to the suspension and the mixture was stirred at room temperature overnight under an inert atmosphere. The GHN-TGE functionalized powder was filtered and washed several times with THF, water and then ethanol. The product was dried in vacuum at 60 °C prior to storage.

2.5. Functionalization of GHN (GHN-GPTMS-TGE / GHN-TGE-GPTMS). A surface functionalization of GHN was carried out with both GPTMS and TGE going step by step. For this, GHN-GPTMS was post-functionalized by TGE and vice versa GHN-TGE by GPTMS in the same conditions as in the case of mono functionalization.

2.6. Ring opening *of the* epoxide modified GHN (GHN-COOH). Since the sample GHN-GPTMS-TGE exhibited a higher grafting density of epoxy groups than GHN-TGE-GPTMS, it was selected for further experiments. Thus, for its transformation to nanomaterial bearing carboxylic acid complexing groups; first, 100 mg of GHN-GPTMS-TGE were dispersed in 5 mL of sulfuric acid (0.1M) with constant stirring then filtered and washed thoroughly with water. Thereafter, the collected GHN-OH nanomaterial was dispersed in 5 mL of a solution of sulfuric acid (0.1M) containing 20 mg of potassium permanganate for 4 hours at room temperature. The obtained nanostructure (GHN-COOH) was filtered, washed with water to remove residuals, and dried at 60 °C under vacuum overnight.

2.7. Immobilization of palladium nanoparticles (GHN-COO@PdNPs). GHN-COO@PdNPs nanohybrid was prepared by a rapid and easy process. Initially, GHN-COOH was subjected to alkaline treatment by sodium hydroxide solution (0.1M) to deprotonate the carboxylic acid functions. Subsequently, the product (GHN-COO^-) was collected without washing and added to 5 mL of an aqueous $PdCl_2$ solution (10^{-2} M). The mixture was stirred overnight at room temperature. Then, 10 ml of $NaBH_4$ solution (0.1 M) was added dropwise to

the suspension and the reaction was allowed to proceed for 1h under stirring. The product was recovered by filtration, washed several times with water and then dried at 60 °C under vacuum.

2.8. Materials characterization. The graphitic structure of GHN sample was studied by alpha 300R confocal Raman microscope with a wavelength of 532 nm. The spectra were recorded using Vitec software.

The microstructure and the elemental mapping of GHN were recorded by a SU8230 model scanning electron microscope (SEM, Hitachi) operated at 10 kV equipped with an Oxford energy dispersive X-ray spectrometer detector (EDS). Morphology and chemical composition of GHN-COO@PdNPs nanohybrid was investigated with a MERLIN microscope integrated with an energy dispersive X-ray spectrometer (SEM-EDX) from Zeiss equipped with InLens and SE2 detectors using an accelerating tension of 20 kV with a diaphragm aperture of 30 µm. Prior to analyses, the samples were coated with a sputtered layer of platinum using a Cressington 208 HR sputter-coater.

Thermal characterization was performed on a Pyris Diamond TGA Perkin Elmer instrument by heating the samples from 25 °C to 800 °C at 10 °C.min^{-1} under pure N_2 atmosphere.

To further characterize the synthesized nanohybrids, structural analyses were accomplished through X-ray diffraction measurements (XRD) and X-ray photoelectron spectroscopy (XPS) technics. XRD analysis of the GHN-COO@PdNPs hybrid catalyst was carried out on a Bruker D8 advance diffractometer. The XRD spectra of the powdered sample was recorded in the 10° - 90° angle range using Cu Kα (λ = 1.54 Å) radiation.

The XPS characterization was conducted for elucidating surface composition/elemental chemical states of the prepared nanohybrid materials. The spectra were recorded using Thermo Scientific K-Alpha spectrometer equipped with a monochromatic Al-Kα X-ray source (hν = 1486 eV, spot size = 400 µm, pass energy of surveys = 200 eV and of narrow regions = 50 eV), and magnetic lens enables analysis of small areas with increased sensitivity. The charge compensation was provided by a combination of an electron flood gun with an argon ion gun. The collected spectra were analyzed by using Advantage software. C1s/O1s atomic ratios were calculated from the intensity of C1s and O1s peaks in survey spectra, multiplied by sensitivity factors (C1s = 1 and s O1s = 2.75).

UV-Vis absorption spectra were recorded at room temperature in real time using an Agilent Cary 60 UV-vis spectrophotometer, where the measurements were performed directly in 3 mL quartz cuvettes between 200-800 nm.

2.9. Evaluation of catalytic activity of GHN-COO@PdNPs. Investigation of the catalytic reduction of methylene blue (MB) and eosin Y (Eo-Y) was carried out using GHN-COO@PdNPs nanohybrid catalysts in the presence of aqueous $NaBH_4$ as a reductant at room temperature. In a typical procedure, nanohybrid catalyst (1 mg) was dispersed in deionized H_2O (1 mL). Then, 0.1 mL of MB or Eo-Y dye solution (1 mM) and 0.1 mL of a freshly prepared aqueous solution of $NaBH_4$ (25 mM) were added. At once, the reaction mixture was placed under continuous stirring into the spectrophotometer to monitor progress of the reduction reaction. UV-vis spectral analysis (Cary 60 spectrophotometer) was performed in the scanning range of 200-800 nm to monitor the catalytic performance of GHN-COO@PdNPs nanohybrid.

For the evaluation of the catalytic performance of synthetized nanohybrids, control tests for the reduction of MB and Eo-Y were performed. Before starting the reduction experiments, on the one hand, to estimate the adsorption capacity of nanohybrids, UV-vis spectra were recorded for the dye solutions in the presence of the catalysts without addition of $NaBH_4$. On the other hand, the UV-vis spectra of the dye solutions were recorded in the absence of nanohybrids in order to evaluate the contribution of $NaBH_4$ in the total reduction reaction. The reusability experiments were achieved by reuse of the nanohybrids catalyst several times in the same reaction conditions. After completion of each reaction, the GHN-COO@PdNPs nanohybrid catalyst was separated out by centrifugation, then washed with deionized water and dried at 60°C under vacuum for the following runs. The reusability efficiency of the nanohybrid catalyst was evaluated by comparison of the values of the apparent reaction rate constants (k_{app}) of the different consecutive cycles. All the experiments were performed in triplicate and the average values of absorbance (A) were considered for kinetic studies.

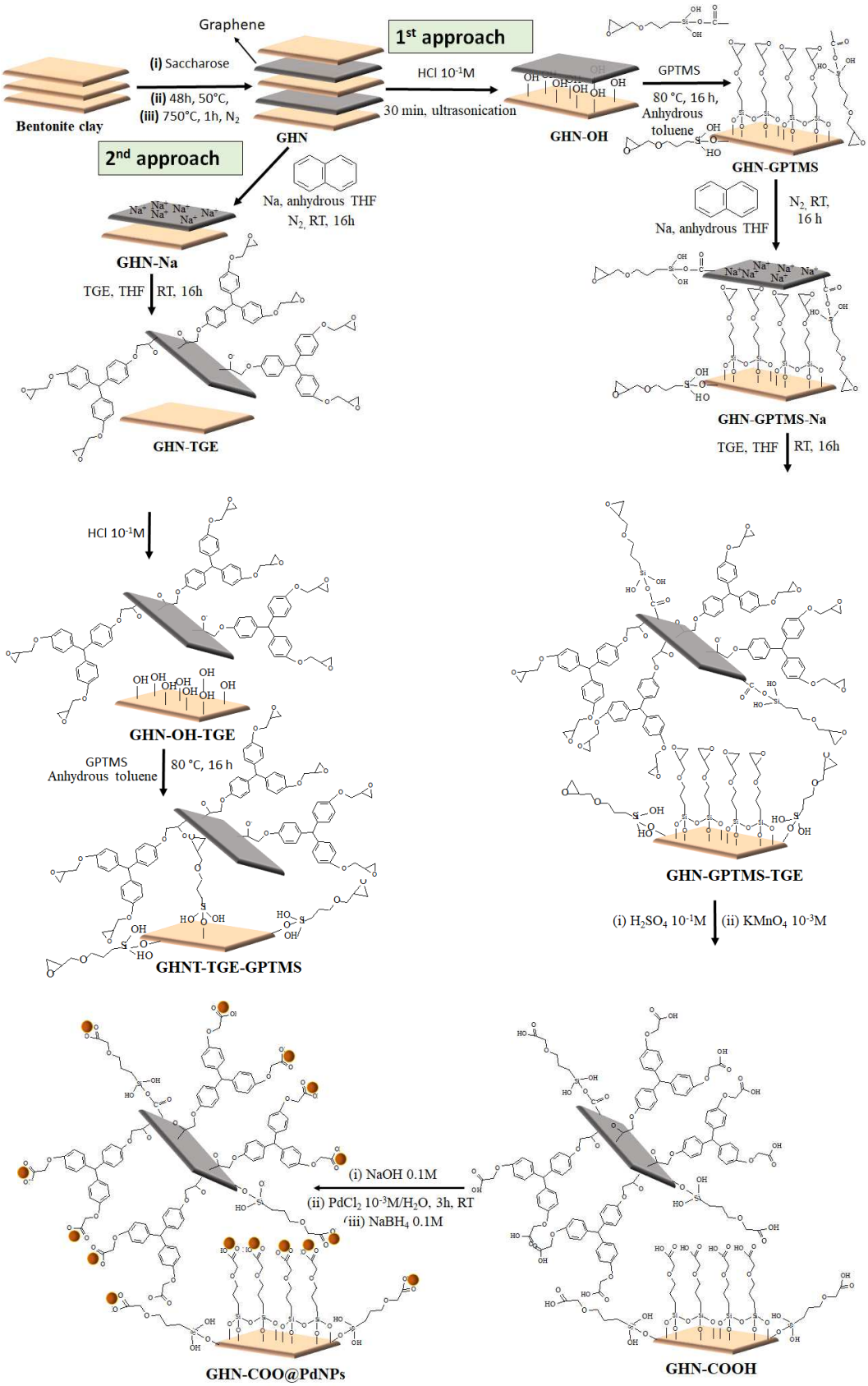

Scheme 1. Schematic representation of the steps for the preparation of supported palladium nanoparticles using graphene like nanomaterial synthesized by a green method via natural precursors. For the sake of clarity, we present the functionalization of only one layer of graphene or clay.

3. RESULTS AND DISCUSSION

3.1. Preparation and characterization of GHN. The pyrolysis technique is recognized as a green and low-cost synthesis method, which has increased significantly its use in practical applications especially for the generation of carbonaceous materials from biomass. [21, 40] Indeed, using this technique, graphene-like materials were successfully prepared on sand [41] and clays [42-43], using saccharose as a source of carbon .[44] Such graphene originated from natural resources has been shown to be promising in various applications such as adsorption of pollutants, energy storage, and reinforcing of polymers. Here, with the aim of using graphene-like nanomaterial (GHN) derived from saccharose through pyrolysis using bentonite clay as a template, to stabilize catalytic palladium nanoparticles, it required functionalization with chelating surface modifiers. Thus, GHN was first functionalized with (3-glycidyloxypropyl) trimethoxysilane (GPTMS) and in a second step with tris (4-hydroxyphenyl) methane triglycidyl ether (TGE). The as-obtained GHN nanomaterial bearing epoxy groups was then subjected to treatment with H_2SO_4/ $KMnO_4$ in order to convert the surface grafted epoxy reactive groups to carboxylic acid ones used finally to in-situ generate PdNPs from previously complexed Pd^{2+} ions on the surface of GHN-COO^- using $NaBH_4$ as reducing agent. The experimental procedure is presented in detail in scheme 1.

The graphitic nature of the synthesized GHN is confirmed by the Raman analysis in Figure 1a. An intense peak at around 1350 cm^{-1} (D band) corresponds to the sp^3 carbon atoms of disordered graphene sheets and a second less intense peak near 1570 cm^{-1} (G band) is attributed to the in-plane vibration of sp^2 carbon atoms. The smaller peak appearing at higher wavenumber (~2750 cm^{-1}) is also a sp^2 Raman signature. Both G and 2D bands reflect the crystalline structure of graphitic carbon.[45] It is observed that the amorphous carbon reflected by the D band is prominent which means a high defect level.[46] To evaluate the disorder of GHN, the ratio of the D to G peak intensities (I_D/I_G) is calculated (~ 1.1) suggesting a partial amorphous nature of GHN resulting from its oxidation. [47-49] It was reported that during the oxidation reaction, disordered sp3-oxidized domains with various oxygen functional groups (such as epoxides, ketones, hydroxyls, carboxylic acids, …) could surround the sp2 graphitic domains.[50]

The XPS survey and high-resolution of the C1s region of GHN are shown in Figure 1b. The survey spectrum shows the co-existence of Al2p, Si2p, Al2s, Si2s, O1s, and Na1s clay constituting atoms centered at around 74.4, 102.7, 119.5, 152.8, 533.4, and 1072 eV,

respectively. It also exhibits strong peak at 284.4 eV assigned to C1s, evidencing the presence of graphene sheets (a carbonaceous nanomaterial) on the surface of bentonite layers.

The C1s spectrum of GHN is fitted with four peak components attributed to the Csp2 (C=C) and Csp3 (C-C /C-H) centered at 284.4 eV, the C-O from epoxide and alcohol groups (C-O-C/C-OH) at 286.2 eV, the carboxyl groups (HO-C=O) at 288.3 eV and π–π* transition satellites at 290 eV; which is in full accordance with the Raman results.

Thermal stability of GHN nanomaterial is investigated by TGA analysis and compared to each precursor (clay and saccharose). An important variation in weight loss is observed as shown in Figure 1c The bentonite curve presents three separated stages corresponding to the dehydration below 150 °C, the elimination of the water coordinated to the interlayer cations (at higher temperature) and the dehydroxylation (above 500 °C). [51] The thermal profile of saccharose exhibits three phases corresponding to the evaporation of the surface adsorbed moisture (~ 100 °C), the decomposition of hydroxyl groups and liberation of CO, CO_2 and H_2 (from 209 °C to 340 °C) and the 100% weight loss between 322 and 558°C. [52] The thermal decomposition of GHN occurred in four stages: (i) desorption of the interlayer water (< 150 °C), (ii) liberation of oxygen functional groups in the temperature range of 150-400 °C, (iii) oxidation of the carbon skeleton of graphene between 400 and 700 °C, and (iv) dehydroxylation of the structural O-H groups in the temperature range of 700-800 °C. [53-54] It is observed that the total mass loss of GHN nanomaterial is 60 % which is located between that of its starting materials, namely clay and saccharose. This suggests the existence of a strong attachment between clay and graphene due to the hydrogen bonds formed between hydroxyl groups of bentonite clay with that coming from -OH and -COOH groups of graphene.

The microstructure and the elemental mapping of GHN are shown in Figures 1-d (1-7) and 1-f clearly substantiate the formation of a graphene/clay composite material. The elemental mapping indicates the presence and the homogeneous distribution of C, O, Mg, Al, Na, Si and Fe in the hybrid nanomaterial. Carbon is mainly originated from graphene, oxygen comes from both clay and graphene as a result of its oxidation while other elements are originated from bentonite clay with a predominant amount of Si (19.6 % of total mass) compared to the other elements of clay. The graphitic nature of GHN and the presence of exogenous groups are also confirmed by the high proportion of carbon (~ 50.5% of the total mass) in line with XPS results. The SEM image of GHN highlights its layered structure consisting of a superposed arrangement of graphene and clay nanosheets. This result is in line with previous study. [55]

In addition, the above statements were supported by the BET surface area measurements based on nitrogen adsorption. Indeed, the specific surface area of GHN (S_{BET} = 266.9 m^2/g) was found to be three times higher than that of BT (87.4 m^2/g). This can be explained by the nano-sandwich structure of GHN formed from graphene and bentonite layers.

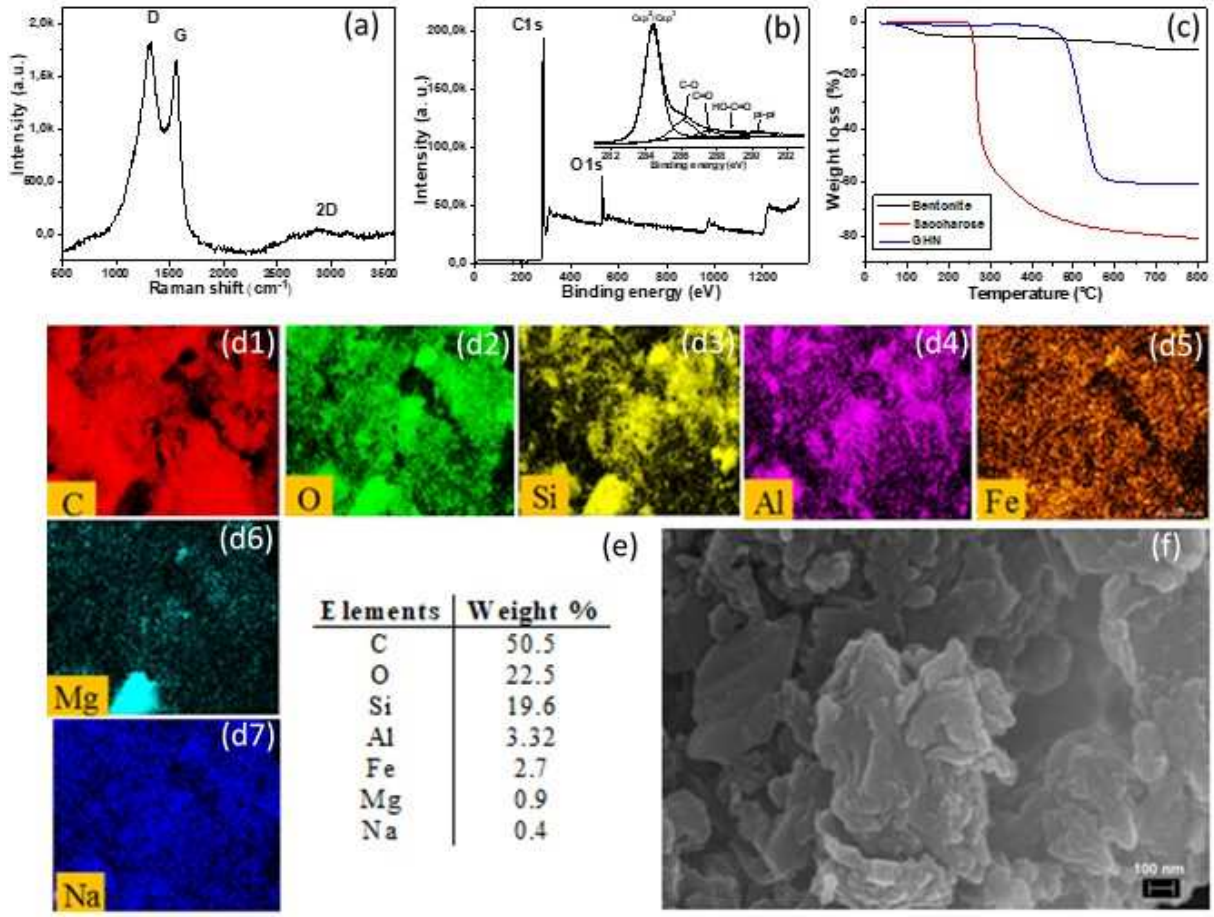

Elements	Weight %
C	50.5
O	22.5
Si	19.6
Al	3.32
Fe	2.7
Mg	0.9
Na	0.4

Figure 1. (a) Raman spectrum, (b) XPS survey scan and C1s high-resolution region (inset), (c) TGA curves of bentonite, saccharose, and GHN, (d1-7) Elemental mapping of the SEM image of GHN, (e) EDS Table showing the elemental composition of GHN, and (f) SEM image of GHN**.**

3.2. Surface functionalization of GHN. The surface modification of GHN plays a dual role as it facilitates the separation of the clay and graphene layers from each other thus preventing their aggregation and imparts appropriate functional groups to the GHN to enable stabilization and well-dispersion of metallic nanoparticles. These properties can easily be tuned by varying both the surface modifiers nature and their grafting density. In this work, two surface modifiers (GPTMS and TGE) containing both epoxy groups were used for a two-step surface functionalization of GHN using two different strategies: (*i*) first, GPTMS and TGE were grafted

separately on GHN and (*ii*) the obtained GHN-GPTMS and GHN-TGE samples were doubly functionalized by TGE and GPTMS, respectively.

To testify their grafting on the surface of clay and graphene layers of GHN, detail information about the surface chemical surface composition of the different samples was obtained by XPS analysis providing full evidence for the presence of the functional groups.

Figure 2a shows a comparison of the survey spectra of pristine and functionalized GHN. All spectra show the presence of both clay and graphene related elements the same as those detected in pristine GHN, confirming that the structure of GHN was preserved upon functionalization. In addition, both C1s (~284 eV) and O1s (~532 eV) peaks intensities in all functionalized GHN samples are much higher comparing to the C1s and O1s in pristine GHN, providing strong evidence for the grafting of molecules rich in carbon and oxygen on the surface of GHN; namely GPTMS ($C_9H_{20}O_5Si$) and TGE ($C_{15}H_{19}NO_4$). The detail of surface composition calculated from the survey spectra is given in the inset of Figure 2a. The differences between the values of O1s/C1s atomic ratios of each functionalized GHN reveal that the degree of surface functionalization was varied as a function of the nature of the surface modifier as well as their order of grafting when two epoxy-containing molecules were used. From these results, one can notice that the degree of functionalization varied in the following order: GHN-TGE < GHN-TGE-GPTMS < GHN-GPTMS < GHN-GPTMS-TGE. For better understanding of chemical changes occurring upon GPTMS and TGE grafting, C1s high-resolution spectra depicted in Figures 2 b-f were investigated and as it can be seen evident differences are exhibited between spectra profiles. The deconvolution of the C1s spectrum of GHN-GPTMS is fitted with four peak components centered at 283, 284.8, 286 and 288.2 eV attributed to C-Si, $C_{sp2}/C_{sp3,}$ C-O-C (ether/epoxide) and C-O-Si/O-C=O groups, respectively, in agreement with the chemical structure of GPTMS at the surface of the GHN nanomaterial. For GHN functionalized with TGE, the C1s spectrum could be deconvoluted into three peaks centered at 284.4, 286.2 and 288.4 eV assigned to C_{sp2}/C_{sp3}, C-O-C (ether/epoxy) and O-C=O (ester and carboxylic acid), respectively. All these results confirmed the presence of GPTMS and TGE on the surface of GHN samples. However, one can notice that the contribution of C-O-C component of GHN-GPTMS is larger than that of GHN-TGE. This can probably be explained by the fact that the GPTMS silane coupling agent can bind to both edges and internal surface of clay and graphene layers while TGE can only be grafted onto graphene (as carbonaceous material).

A comparison between C1s spectra of GHN-GPTMS-TGE with GHN-TGE-GPTMS revealed that the degree of grafting is largely higher in the case where GHN was first treated with

GPTMS then with TGE, indicating an enhanced C-O-C epoxy component at ~ 286 eV in accordance with the higher O1s/C1s ratio of GHN-GPTMS-TGE than GHN-TGE-GPTMS (inset of Figure 2a). This marked difference can be explained by the interlayer spacing enlargement of graphene and clay after grafting of GPTMS which facilitates the penetration of TGE molecules in between the layers and thus their grafting. In contrast, when TGE was used first, the grafting density is low as shown above, which results in poor dispersion of GHN-TGE. In addition, the hydrophobic nature of TGE molecules limits the accessibility of GPTMS entities to the internal surface of graphene and clay.

After treatment of GHN-GPTMS-TGE successively with H_2SO_4 and $KMnO_4$, significant changes can be detected in the chemical structure of the GHN as shown in Figures 2a and 2f. Indeed, a strong decrease of the intensity of the component at 286.1 eV associated with C-O-C of the epoxide groups is observed due to their conversion to carboxylic acid functions via ring opening reaction. The C1s spectrum shows that GHN-COOH contains C-Si (283 eV), Csp^2/Csp^3 (284.3 eV), C-O-C (286.1 eV), and C-O-Si/O-C=O (288.8 eV).

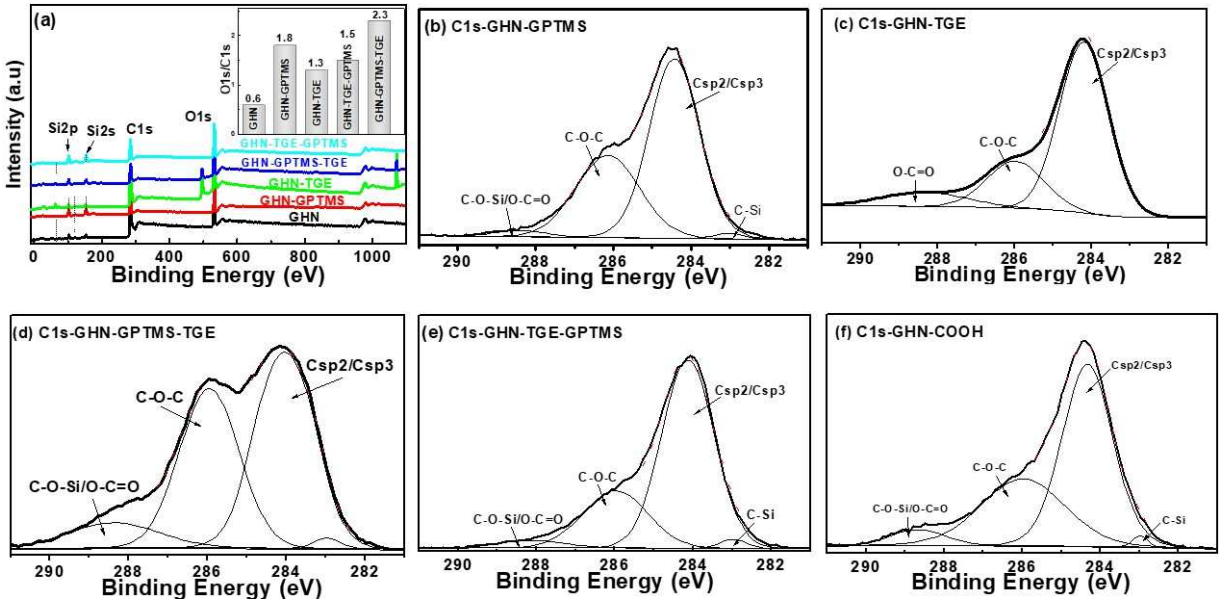

Figure 2. XPS survey (a) and C1s high-resolution spectra of (b) GHN-GPTMS, (c) GHN-TGE, (d) GHN-GPTMS-TGE, (e) GHN-TGE-GPTMS, (f) GHN-COOH prepared by conversion of epoxy groups of GHN-GPTMS-TGE to carboxylic acid ones. Inset: atomic fraction and values of O1s/C1s rations of pristine and all functionalized GHN samples.

3.3. Palladium nanoparticles decorated GHN. The functionalized GHN nanohybrid contains large amount of carboxylic acid moieties at the surface, allowing palladium nanoparticles to

grow and bind to the GHN layers since COO^- functional group is an effective complexing agent for divalent cations, such as Pd^{2+}. [25]

SEM analysis is carried out to evaluate the distribution and dispersion state of palladium nanoparticles generated on the surface of the carboxylate-rich GHN nanohybrid. Figure 4a clearly shows that the surface of the layered nanohybrid material was fully covered with homogeneously and uniformly distributed ultrasmall PdNPs with an average diameter around 4.5 nm as shown in the inset of Figure 3a. Energy dispersive X-ray analysis (EDX) was used to identify the elemental composition of the nanohybrid. The EDX spectrum shown in Figure 3b revealed a signal of palladium centered at 2.85 eV with an estimated amount around 14 wt.%. The dense covering of the surface of GHN with PdNPs is indicative of the effectiveness of the surface functionalization.

The SEM/EDX results were supported by XRD characterization, as shown in Figure 3c. The typical pattern of GHN-COO@PdNPs presents different planes of this nanomaterial.[56] While, the peaks at about 2Θ = 39.95, 46.16, 68 and 81.5° are related to the (111), (200), (220) and (311) diffraction peaks for face-centered-cubic structure palladium crystals[57], demonstrating that the palladium nanoparticles were successfully in-situ generated on the surface of GHN nanohybrid. It is noteworthy that the narrow and intense peak observed at 2Θ = 26,5° corresponding to the diffraction from (002) plane, confirms that the ordered structure of GHN was preserved.

To provide information about the nature of the palladium generated on the deprotonated GHN-COOH nanomaterial, XPS was performed and the result is shown in Figure 3d. We can obviously detect a metallic Pd 3d contribution. Indeed, intense spin-split doublet peaks are displayed at binding energies centered at 335.6 and 340.7 eV assigned to $3d_{5/2}$ and $3d_{3/2}$ electronic state of zero valent palladium, respectively, confirming the successful formation of PdNPs on the surface of GHN. In addition to Pd (0), shoulders of the main peaks are also detected at higher binding energies values of 337 and 343 eV, characteristic of the Pd (II) ions, which can be explained by the oxidation of a small amount of PdNPs to form PdO NPs. These results are close to those reported in the literature for supported palladium nanoparticles. [58]

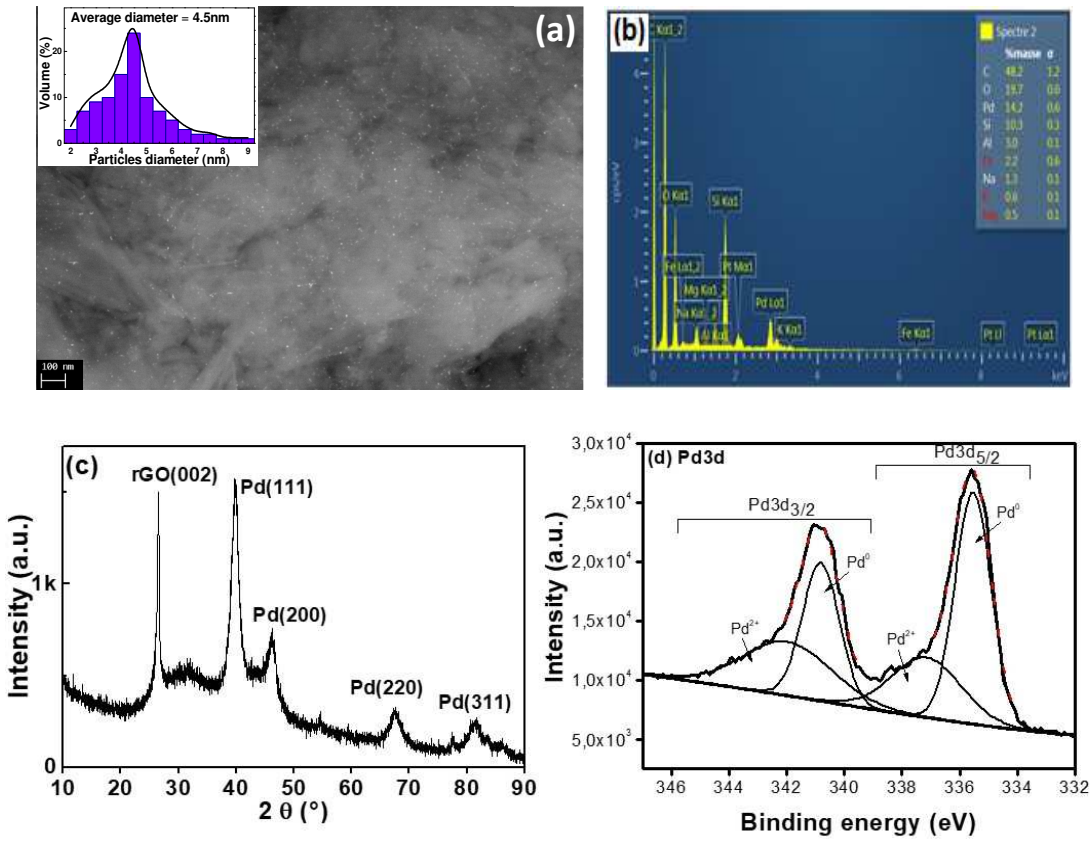

Figure 3. GHN-COO@PdNPs (a) SEM image (inset: PdNPs size distribution), (b) EDS spectrum (inset: elemental composition), (c) XRD pattern.and (d) Pd 3d high-resolution XPS spectrum.

3.4. Catalytic properties of GHN-COOH@PdNPs. The catalytic activity of the palladium nanoparticles-decorated hybrid nanomaterial was evaluated in batch process on the reduction of methylene blue (MB) as cationic organic dye and eosin Y (Eo-Y) applied as model anionic organic dye and in the presence of $NaBH_4$ as reducing agent. Firstly, control experiments were carried out to rule out the possibility of the adsorption of the studied dyes on the GHN-COOH@PdNPs nanohybrid as well as their reduction by $NaBH_4$ in the absence of catalysts. The obtained real time UV-vis spectra are shown in Figure 4. For this, an amount of 1 mg of GHN-COOH@PdNPs was dispersed under magnetic stirring in 1 mL of water before mixed with dye solutions. Additionally, the adsorption of the same dyes on the nanohybrid was studied without introducing $NaBH_4$ and the absorbance variation was monitored by time-dependent UV-vis spectrophotometry. The experimental results show a slight decrease of the intensities of absorption peaks of MB (16.6%) and Eo-Y (20.8%) but no visible change of the initial dye solution colour was observed after 24 h of contact time. The slight decrease of the characteristic absorption peaks is due to adsorption of the dye molecules onto the functionalized GHN layers via π-π interactions and hydrogen bonds. [59-61] Furthermore, when the dye solutions were mixed with freshly prepared aqueous solutions of $NaBH_4$ in the absence of the immobilized PdNPs

nanocatalyst, a very low decrease of the characteristic absorption peaks at 666 nm (30.1-16.6=13.5%) and 517 nm (22.4-20.8=1.6%) corresponding respectively to MB and Eo-Y occurred. These investigations showed that in the absence of PdNPs decorated GHN, very slow and slight decrease of the intensity of the characteristic peak of each dye was observed even after a long time (24h) indicating that the reduction reaction did not occur (very low yield of the reduction reaction was reached).

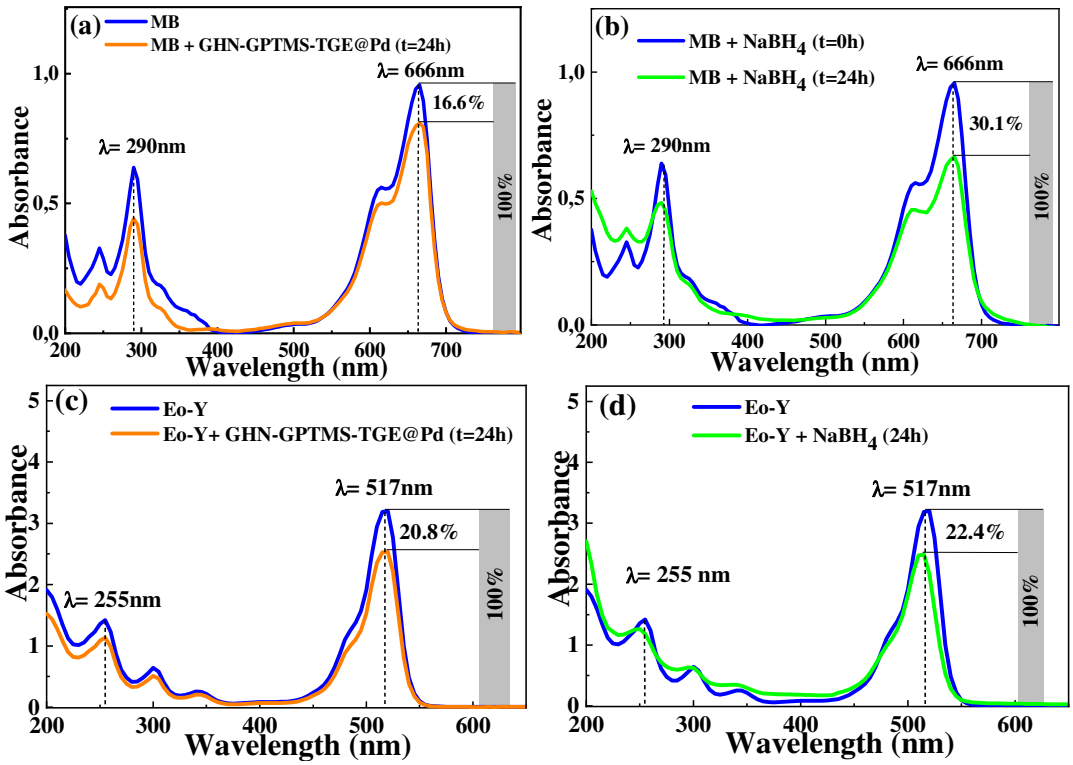

Figure 4. (a and c) UV-vis absorption spectra of pure (blue) MB and Eo-Y, and (red) 24h after addition of GHN-COO@PdNPs nanocatalyst without $NaBH_4$, respectively. (b and d) UV-vis absorption spectra of pure (blue) MB and Eo-Y, and (green) 24h after addition of an excess $NaBH_4$ without catalyst, respectively. Reaction conditions: [Dyes] = 0.1 mM, [$NaBH_4$] = 25 mM, [GHN-COO@PdNPs] = 0.25 g/L.

To investigate the catalytic activity of the GHN-COOH@PdNPs nanohybrid, a higher $NaBH_4$ concentration of 25 mM was used as compared to that of dyes ([MB] = [Eo-Y] = 0.1 mM). The catalytic reduction, at room temperature, of dye solutions was carried out by introducing 1 mg of nanohybrid catalyst in the dyes/$NaBH_4$ solution mixture.

The recorded real time UV-Vis spectra (Figures 5 a-b) showed a rapid decrease in the intensity of the maximum absorption band (λ_{max}) at 666 nm and 517 nm of MB and Eo-Y dye solutions, respectively. The catalytic conversion was found to be complete and rapid in the presence of immobilized PdNPs. Based on these results, we can conclude that their presence on

the surface of GHN is the key feature which contributes to achieve a total conversion with a fast reaction rate. The reduction process was achieved by the electron's transfer from the BH_4^- anions with high nucleophilicity to the dyes through the surface of the immobilized PdNPs which play the role of electron reservoir redox catalyst and this by acting as electron relay system.[62] Firstly, functionalized GHN adsorbs the dye molecules through π-π interactions and hydrogen bonds as demonstrated above, which increases their concentrations into the nanohybrids and favor the close vicinity of the dye molecules on the immobilized PdNPs surface.[62-63] Subsequently, the diffusion of both dyes and BH_4^- anions to the surface of the PdNPs occurred. Then, the electrons generated from the oxidation of BH_4^- anions are rapidly transferred to dyes mediated by the catalyst surface thereby allowing to reduce their activation energy and thus accelerate the reduction reaction.[63] Figures 5a and 5b represent the UV-Vis spectra for the reduction of MB and Eo-Y, respectively, by $NaBH_4$ in the presence of GHN-COO@PdNPs nanocatalyst recorded every 30 s to track the reaction progress. It was found that the catalytic reduction of dyes happened immediately and the intensity of the characteristic UV-Vis absorption spectra of MB (666 nm) and Eo-Y (517 nm) vanished within 240 s and 420 s, respectively. Accordingly, a total decolorizing of dye solutions at the end of the reaction was observed (see photographs of Figure 5d) revealing the complete destruction of chromophoric structure of the MB and Eo-Y by the reduction of their double bonds to single bonds. Moreover, a linear correlation between $\ln(A/A_0)$ versus reaction time (in second); with 'A' is the absorbance at time 't' after the addition of the nanocatalyst and 'A_0' is the initial absorbance before the addition of the nanocatalyst; was established in the degradation reaction of the two dyes and the kinetic data were fitted by a pseudo-first-order reaction. The reaction rate constants k_{app} for MB and Eo-Y dyes reduction were calculated from the plot of $\mathrm{Ln}(A/A_0)$ versus time and were found to be equal to 1.65×10^{-2} and 0.93×10^{-2} s^{-1}, respectively (Figure 5c).

These results proved that the $NaBH_4$ alone is insufficient to reduce the dyes and this requires the presence of a catalyst to accelerate the kinetics of the reaction as it has been already demonstrated.[62-63] Indeed, it is important to highlight the crucial role of the palladium nanoparticles which act as mediator surface for electrons transfer from BH_4^- donor species to the dyes acceptor molecules [62, 64], which favor the kinetic reduction of dyes as shown in Figures 5c and 5d.

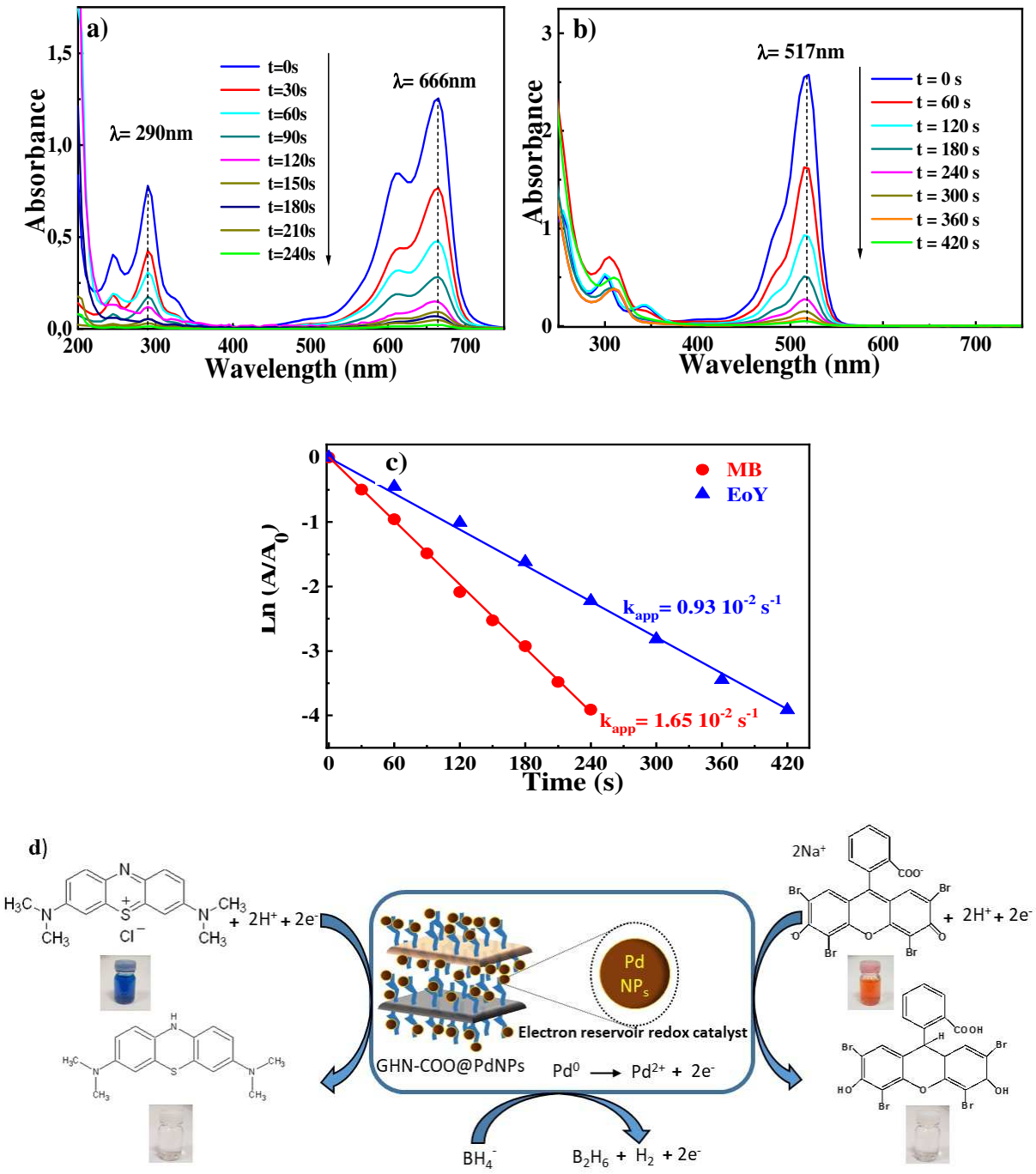

Figure 5. Time-dependent of UV–vis absorption spectra showing the gradual reduction of a) MB and b) Eo-Y. c) Plots of ln(A/A_0) versus reaction time for pseudo-first-order reaction for the reduction of MB and Eo-Y at room temperature by using excess $NaBH_4$ in the presence of GHN-COO@PdNPs as catalysts. Reaction conditions: [Dye] = 0.1 mM, [$NaBH_4$] = 25 mM, [GHN-COO@PdNPs]=0.25 g/L. d) Proposed mechanism of the reduction of MB, and Eo-Y organic dyes by PdNPs immobilized on GHN-COOH nanohybrid with excess of $NaBH_4$.

In order to evaluate the benefits of the synthetic approach developed in our work, the catalytic performance of the PdNPs decorated carboxylate-rich graphene-like nanomaterial was compared to those reported in literature. As seen in the Table 2, the nanohybrid catalyst synthesized in our work exhibits an excellent catalytic efficiency compared to other reported

Pd catalysts for the reduction of organic dyes. This high catalytic activity could be attributable to three main reasons. Firstly, the homogeneous Pd NPs loading on the two-dimensional graphene-like nanomaterial surface allows for a high surface area for efficient complexing the dye molecules. [59, 63] Secondly, the organic functionalization process of the GHN surface leads to a greater stabilizing of PdNPs and inhibits the aggregation of the small-sized nanoparticles. [65-66] thirdly, the good dispersion of the nanohybrid catalyst (GHN-COO@PdNPs) in water provides a highly efficient contact between the catalytic sites (Pd NPs) and the exposed dye molecules. [62, 67]

These three factors result in a very high reduction rate with respect to the previously reported ones. Interestingly, this work demonstrates a facile and efficient approach for preparing supported Pd nanocomposites as well as its great benefices in the catalytic reduction of hazardous dyes solutions. Finally, the synergistic effects between the Pd NPs and the silane modified graphene oxide structure makes of our nanohybrid catalyst a promising candidate for more wide catalysis applications. [49, 68]

Table 2. Comparison of literature results obtained with PdPNs catalysts for the reduction of various dyes.

Catalyst	Dye molecule	k_{app} (10^{-2} s^{-1})	Time (min)	Reference
$Pd_{75}Au_{25}$/Dens-OH	MO	0.587	3.5	69
GO/Pd nanocomposite			5	70
Natrolite zeolite/Pd nanocomposite			5	71
Pd-PEI-RGO	MB	0.74	6	62
Pd-TNPs/RGO nanohybrid		0.66	7	72
PDA-RGO/Pd		0.4	13	60
Pd NPs/Fe_3O_4-PEI-RGO nanohybrids	MO R6G RB	-	10	28
Si/Pd catalyst	Eo-Y	0.11	20	73
GO/Pd NCs	CV	0.48	-	74
GO/Ru-Pd NCs		0.55	-	
GO/Pd NCs	MG	0.47	-	
GO/Ru-Pd NCs		0.54	-	
GHN/Pd nanocomposite	MB	1.65	4	This work
	ALZ	1.6	3.5	
	Eo-Y	0.93	7	

3.5. GHN-COOH@PdNPs Catalyst regeneration. Although GHN-COOH@PdNPs promoted a great catalytic efficiency, it is vital to assess the nanocatalyst stability as an

influencing factor in practical applications. Therefore, recyclability of this nanocatalyst in the catalytic reduction of MB (10^{-4}M) in presence of $NaBH_4$ was chosen as model reaction and was investigated for 8 consecutive cycles. At the end of each reduction run, the nanohybrid catalyst was readily separated from the reaction mixture by centrifugation, washed with water and ethanol, and further dried under vacuum. By comparing the degradation rates calculated for eight reduction cycles, no significant change in the reduction activity is found, also the catalyst exhibited similar apparent rate constants, as shown in Figure 7. Therefore, the high catalytic performance, the great stability and the easy recycling make the GHN-COO@PdNPs nanohybrid material a very competitive for catalyst =for environmental remediation.

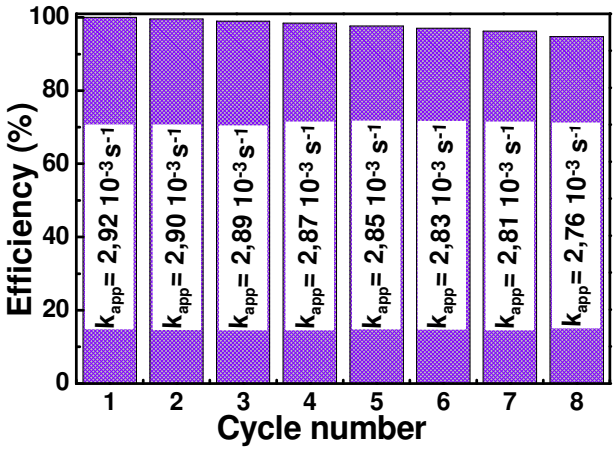

Figure 7. Reusability of GHN-COO@PdNPs catalyst for the reduction of MB with $NaBH_4$ for 8 cycles.

4. CONCLUSION

In summary, covalent surface functionalization of graphene-like nanomaterial (GHN) prepared from natural precursors with two epoxy-containing molecules was reported for the first time. GHN was generated from saccharose as a carbon source in the presence of bentonite clay layers using pyrolysis method. Subsequent functionalization of GHN by two different epoxy-containing molecules, namely GPTMS and TEG, followed by ring opening of the epoxy reactive groups *via* an oxidation reaction by H_2SO_4/KnO_4, allowed for the introduction of a high density of carboxylic acid functions onto the GHN surface. The as-designed GHN-COOH nanohybrid was first deprotonated using NaOH solution and then used as support for complexation of Pd^{2+} ions to finally in-situ reduce them to palladium nanocrystals using $NaBH_4$

as a mild reducing agent. The GHN-COO@PdNPs nanohybrid exhibits excellent catalytic performance in the reduction of both cationic (MB) and anionic (Eo-Y) toxic organic dyes in aqueous solution and can be recycled for at least 8 consecutive cycles while retaining its catalytic activity. All these beneficial features result from the high stabilization of the PdNPs on the GHN-COOH platform induced by the strong interaction between the PdNPs and the grafted carboxylic acid groups. Due to the well-known versatility of epoxy groups, the sustainable strategy proposed here can straightforwardly be used to prepare various heterogeneous catalysts by incorporating desired chelatant moieties onto epoxy decorated GHN and hence use them as selective supports for a high variety of catalytic metal nanoparticles.

Declaration of Competing Interest

There are no conflicts to declare

REFERENCESUncategorized References

(1) Bashir, B.; Rahman, A.; Sabeeh, H.; Khan, M. A.; Aboud, M. F. A.; Warsi, M. F.; Shakir, I.; Agboola, P. O.; Shahid, M. Copper substituted nickel ferrite nanoparticles anchored onto the graphene sheets as electrode materials for supercapacitors fabrication. *Ceramics International* **2019,** *45* (6), 6759-6766.

(2) Zhang, Y.; Liu, S.; Wang, L.; Qin, X.; Tian, J.; Lu, W.; Chang, G.; Sun, X. One-pot green synthesis of Ag nanoparticles-graphene nanocomposites and their applications in SERS, H 2 O 2, and glucose sensing. *Rsc Advances* **2012,** *2* (2), 538-545.

(3) Rosaiah, P.; Zhu, J.; Shaik, D. P.; Hussain, O.; Qiu, Y.; Zhao, L. Reduced graphene oxide/Mn3O4 nanocomposite electrodes with enhanced electrochemical performance for energy storage applications. *Journal of Electroanalytical Chemistry* **2017,** *794*, 78-85.

(4) Zhao, X.; Li, N.; Jing, M.; Zhang, Y.; Wang, W.; Liu, L.; Xu, Z.; Liu, L.; Li, F.; Wu, N. Monodispersed and spherical silver nanoparticles/graphene nanocomposites from gamma-ray assisted in-situ synthesis for nitrite electrochemical sensing. *Electrochimica Acta* **2019,** *295*, 434-443.

(5) Luo, S.; Zeng, Z.; Zeng, G.; Liu, Z.; Xiao, R.; Chen, M.; Tang, L.; Tang, W.; Lai, C.; Cheng, M.; Shao, B.; Liang, Q.; Wang, H.; Jiang, D. Metal Organic Frameworks as Robust Host of Palladium Nanoparticles in Heterogeneous Catalysis: Synthesis, Application, and Prospect. *ACS Applied Materials & Interfaces* **2019,** *11* (36), 32579-32598.

(6) Shipilova, O. I.; Gorbunov, S. P.; Paperny, V. L.; Chernykh, A. A.; Dresvyansky, V. P.; Martynovich, E. F.; Rakevich, A. L. Fabrication of metal-dielectric nanocomposites using a table-top ion implanter. *Surface and Coatings Technology* **2020,** *393*, 125742.

(7) Singla, R.; Guliani, A.; Kumari, A.; Yadav, S. K. Metallic nanoparticles, toxicity issues and applications in medicine. In *Nanoscale materials in targeted drug delivery, theragnosis and tissue regeneration*; Springer: 2016; pp 41-80.

(8) Dong, Z.; Le, X.; Dong, C.; Zhang, W.; Li, X.; Ma, J. Ni@ Pd core-shell nanoparticles modified fibrous silica nanospheres as highly efficient and recoverable catalyst for reduction of 4-nitrophenol and hydrodechlorination of 4-chlorophenol. *Applied Catalysis B: Environmental* **2015,** *162*, 372-380.

(9) Liang, Q.; Liu, J.; Wei, Y.; Zhao, Z.; MacLachlan, M. J. Palladium nanoparticles supported on a triptycene-based microporous polymer: highly active catalysts for CO oxidation. *Chemical Communications* **2013,** *49* (79), 8928-8930.

(10) Dutta, D.; Phukan, A.; Dutta, D. K. Nanoporous montmorillonite clay stabilized copper nanoparticles: Efficient and reusable catalyst for oxidation of alcohols. *Molecular Catalysis* **2018,** *451*, 178-185.

(11) Chen, Z.; Cui, Z.-M.; Niu, F.; Jiang, L.; Song, W.-G. Pd nanoparticles in silica hollow spheres with mesoporous walls: a nanoreactor with extremely high activity. *Chemical communications* **2010,** *46* (35), 6524-6526.
(12) Kaushik, M.; Moores, A. Nanocelluloses as versatile supports for metal nanoparticles and their applications in catalysis. *Green Chemistry* **2016,** *18* (3), 622-637.
(13) Fang, H.; Zheng, J.; Luo, X.; Du, J.; Roldan, A.; Leoni, S.; Yuan, Y. Product tunable behavior of carbon nanotubes-supported Ni–Fe catalysts for guaiacol hydrodeoxygenation. *Applied Catalysis A: General* **2017,** *529*, 20-31.
(14) Su, D.; Zhang, Y.; Wang, Z.; Wan, Q.; Yang, N. Decoration of graphene nano platelets with gold nanoparticles for voltammetry of 4-nonylphenol. *Carbon* **2017,** *117*, 313-321.
(15) Liu, J.; Ma, Q.; Huang, Z.; Liu, G.; Zhang, H. Recent progress in graphene-based noble-metal nanocomposites for electrocatalytic applications. *Advanced Materials* **2019,** *31* (9), 1800696.
(16) Guo, H.; Li, Z.; Xiang, L.; Jiang, N.; Zhang, Y.; Wang, H.; Li, J. Efficient removal of antibiotic thiamphenicol by pulsed discharge plasma coupled with complex catalysis using graphene-WO_3-Fe_3O_4 nanocomposites. *Journal of Hazardous Materials* **2021,** *403*, 123673.
(17) Zhong, Y.; Mahmud, S.; He, Z.; Yang, Y.; Zhang, Z.; Guo, F.; Chen, Z.; Xiong, Z.; Zhao, Y. Graphene oxide modified membrane for highly efficient wastewater treatment by dynamic combination of nanofiltration and catalysis. *Journal of Hazardous Materials* **2020,** *397*, 122774.
(18) Guo, Y.; Yang, X.; Ruan, K.; Kong, J.; Dong, M.; Zhang, J.; Gu, J.; Guo, Z. Reduced graphene oxide heterostructured silver nanoparticles significantly enhanced thermal conductivities in hot-pressed electrospun polyimide nanocomposites. *ACS applied materials & interfaces* **2019,** *11* (28), 25465-25473.
(19) Si, Y.; Samulski, E. T. Exfoliated graphene separated by platinum nanoparticles. *Chemistry of Materials* **2008,** *20* (21), 6792-6797.
(20) Şenol, A. M.; Metin, Ö.; Onganer, Y. A facile route for the preparation of silver nanoparticles-graphene oxide nanocomposites and their interactions with pyronin Y dye molecules. *Dyes and Pigments* **2019,** *162*, 926-933.
(21) De Silva, K.; Huang, H.-H.; Joshi, R.; Yoshimura, M. Chemical reduction of graphene oxide using green reductants. *Carbon* **2017,** *119*, 190-199.
(22) Kou, R.; Shao, Y.; Mei, D.; Nie, Z.; Wang, D.; Wang, C.; Viswanathan, V. V.; Park, S.; Aksay, I. A.; Lin, Y. Stabilization of electrocatalytic metal nanoparticles at metal− metal oxide− graphene triple junction points. *Journal of the American Chemical Society* **2011,** *133* (8), 2541-2547.
(23) Silva, M. K. L.; Cesarino, I. Graphene Functionalization and Nanopolymers. In *Graphene Functionalization Strategies*; Springer: 2019; pp 157-178.
(24) Sinha, A.; Chen, J.; Jain, R. Functionalized Graphene-Metal Nanoparticles Nanohybrids as Electrochemical Sensors. In *Graphene Functionalization Strategies*; Springer: 2019; pp 49-62.
(25) Mahouche Chergui, S.; Ledebt, A.; Mammeri, F.; Herbst, F.; Carbonnier, B.; Ben Romdhane, H.; Delamar, M.; Chehimi, M. M. Hairy carbon nanotube@ nano-pd heterostructures: design, characterization, and application in suzuki c− c coupling reaction. *Langmuir* **2010,** *26* (20), 16115-16121.
(26) Sharma, N.; Saha, R.; Parveen, N.; Sekar, G. Palladium-Nanoparticles-Catalyzed Oxidative Annulation of Benzamides with Alkynes for the Synthesis of Isoquinolones. *Advanced Synthesis & Catalysis* **2017,** *359* (11), 1947-1958.
(27) Jin, Z.; Nackashi, D.; Lu, W.; Kittrell, C.; Tour, J. M. Decoration, migration, and aggregation of palladium nanoparticles on graphene sheets. *Chemistry of Materials* **2010,** *22* (20), 5695-5699.
(28) Su, C.; Zhao, S.; Zhang, H.; Chang, K. Ultrafine palladium nanoparticle-bonded to polyetheylenimine grafted reduced graphene oxide nanosheets: Highly active and recyclable catalyst for degradation of dyes and pigments. *Korean Journal of Chemical Engineering* **2017,** *34* (3), 609-618.
(29) Wainwright, M. Dyes in the development of drugs and pharmaceuticals. *Dyes and Pigments* **2008,** *76* (3), 582-589.
(30) Nollet, L. Residues and other food component analysis. *Handbook of food analysis* **2004,** *2*.

(31) Pawlak, K.; Puchalska, M.; Miszczak, A.; Rosłoniec, E.; Jarosz, M. Blue natural organic dyestuffs—from textile dyeing to mural painting. Separation and characterization of coloring matters present in elderberry, logwood and indigo. *Journal of mass spectrometry* **2006,** *41* (5), 613-622.
(32) Hunger, K. *Industrial dyes: chemistry, properties, applications*, John Wiley & Sons: 2007.
(33) Muthu, S. S. *Sustainable Innovations in Textile Chemistry and Dyes*, Springer: 2018.
(34) Tang, X.; Zhou, Y.; Peng, M. Green preparation of epoxy/graphene oxide nanocomposites using a glycidylamine epoxy resin as the surface modifier and phase transfer agent of graphene oxide. *ACS applied materials & interfaces* **2016,** *8* (3), 1854-1866.
(35) Chen, L.; Chai, S.; Liu, K.; Ning, N.; Gao, J.; Liu, Q.; Chen, F.; Fu, Q. Enhanced epoxy/silica composites mechanical properties by introducing graphene oxide to the interface. *ACS applied materials & interfaces* **2012,** *4* (8), 4398-4404.
(36) Martinez-Rubi, Y.; Ashrafi, B.; Guan, J.; Kingston, C.; Johnston, A.; Simard, B.; Mirjalili, V.; Hubert, P.; Deng, L.; Young, R. J. Toughening of epoxy matrices with reduced single-walled carbon nanotubes. *ACS applied materials & interfaces* **2011,** *3* (7), 2309-2317.
(37) Sui, Z.-Y.; Cui, Y.; Zhu, J.-H.; Han, B.-H. Preparation of three-dimensional graphene oxide–polyethylenimine porous materials as dye and gas adsorbents. *ACS applied materials & interfaces* **2013,** *5* (18), 9172-9179.
(38) Mahouche-Chergui, S.; Boussaboun, Z.; Oun, A.; Kazembeyki, M.; Hoover, C. G.; Carbonnier, B.; Ouellet-Plamondon, C. M. Sustainable preparation of graphene-like hybrid nanomaterials and their application for organic dyes removal. *Chemical Engineering Science* **2021**, 116482.
(39) Pénicaud, A.; Poulin, P.; Derré, A.; Anglaret, E.; Petit, P. Spontaneous dissolution of a single-wall carbon nanotube salt. *Journal of the American Chemical Society* **2005,** *127* (1), 8-9.
(40) Kong, X.; Zhu, Y.; Lei, H.; Wang, C.; Zhao, Y.; Huo, E.; Lin, X.; Zhang, Q.; Qian, M.; Mateo, W. Synthesis of graphene-like carbon from biomass pyrolysis and its applications. *Chemical Engineering Journal* **2020**, 125808.
(41) Gupta, S. S.; Sreeprasad, T. S.; Maliyekkal, S. M.; Das, S. K.; Pradeep, T. Graphene from sugar and its application in water purification. *ACS applied materials & interfaces* **2012,** *4* (8), 4156-4163.
(42) Ruiz-García, C.; Pérez-Carvajal, J.; Berenguer-Murcia, A.; Darder, M.; Aranda, P.; Cazorla-Amorós, D.; Ruiz-Hitzky, E. Clay-supported graphene materials: application to hydrogen storage. *Physical Chemistry Chemical Physics* **2013,** *15* (42), 18635-18641.
(43) Azizi, S.; Ouellet-Plamondon, C. M.; Nguyen-Tri, P.; Fréchette, M.; David, E. Electrical, thermal and rheological properties of low-density polyethylene/ethylene vinyl acetate/graphene-like composite. *Composites Part B: Engineering* **2019,** *177*, 107288.
(44) Das, V. K.; Shifrina, Z. B.; Bronstein, L. M. Graphene and graphene-like materials in biomass conversion: paving the way to the future. *Journal of Materials Chemistry A* **2017,** *5* (48), 25131-25143.
(45) Jorio, A.; Dresselhaus, M. S.; Saito, R.; Dresselhaus, G. *Raman spectroscopy in graphene related systems*, John Wiley & Sons: 2011.
(46) Hoepfner, J. C.; Pezzin, S. H. Functionalization of carbon nanotubes with (3-glycidyloxypropyl)-trimethoxysilane: Effect of wrapping on epoxy matrix nanocomposites. *Journal of Applied Polymer Science* **2016,** *133* (47).
(47) Ganguly, A.; Sharma, S.; Papakonstantinou, P.; Hamilton, J. Probing the thermal deoxygenation of graphene oxide using high-resolution in situ X-ray-based spectroscopies. *The Journal of Physical Chemistry C* **2011,** *115* (34), 17009-17019.
(48) Stankovich, S.; Dikin, D. A.; Piner, R. D.; Kohlhaas, K. A.; Kleinhammes, A.; Jia, Y.; Wu, Y.; Nguyen, S. T.; Ruoff, R. S. Synthesis of graphene-based nanosheets via chemical reduction of exfoliated graphite oxide. *carbon* **2007,** *45* (7), 1558-1565.
(49) Zhuo, Q.; Ma, Y.; Gao, J.; Zhang, P.; Xia, Y.; Tian, Y.; Sun, X.; Zhong, J.; Sun, X. Facile synthesis of graphene/metal nanoparticle composites via self-catalysis reduction at room temperature. *Inorganic chemistry* **2013,** *52* (6), 3141-3147.
(50) Hansora, D. P.; Mishra, S. *Graphene Nanomaterials: Fabrication, Properties, and Applications*, CRC press: 2017.

(51) Donoso, J. P.; Tambelli, C.; Magon, C. J.; Mattos, R.; Silva, I.; Souza, J. d.; Moreno, M.; Benavente, E.; Gonzalez, G. Nuclear magnetic resonance study of hydrated bentonite. *Molecular Crystals and Liquid Crystals* **2010,** *521* (1), 93-103.
(52) Eggleston, G.; Yen, J. W. T.; Alexander, C.; Gober, J. Measurement and analysis of the mannitol partition coefficient in sucrose crystallization under simulated industrial conditions. *Carbohydrate research* **2012,** *355*, 69-78.
(53) Gong, J.; Liu, J.; Wen, X.; Jiang, Z.; Chen, X.; Mijowska, E.; Tang, T. Upcycling waste polypropylene into graphene flakes on organically modified montmorillonite. *Industrial & Engineering Chemistry Research* **2014,** *53* (11), 4173-4181.
(54) Ouellet-Plamondon, C. M.; Stasiak, J.; Al-Tabbaa, A. The effect of cationic, non-ionic and amphiphilic surfactants on the intercalation of bentonite. *Colloids and Surfaces A: Physicochemical and Engineering Aspects* **2014,** *444*, 330-337.
(55) Narayanan, D. P.; Gopalakrishnan, A.; Yaakob, Z.; Sugunan, S.; Narayanan, B. N. A facile synthesis of clay–graphene oxide nanocomposite catalysts for solvent free multicomponent Biginelli reaction. *Arabian Journal of Chemistry* **2020,** *13* (1), 318-334.
(56) Qiu, T.; Yang, J.-G.; Bai, X.-J.; Wang, Y.-L. The preparation of synthetic graphite materials with hierarchical pores from lignite by one-step impregnation and their characterization as dye absorbents. *RSC advances* **2019,** *9* (22), 12737-12746.
(57) Saikia, P. K.; Bhattacharjee, R. P.; Sarmah, P. P.; Saikia, L.; Dutta, D. K. A green synthesis of Pd nanoparticles supported on modified montmorillonite using aqueous Ocimum sanctum leaf extract: a sustainable catalyst for hydrodechlorination of 4-chlorophenol. *RSC advances* **2016,** *6* (111), 110011-110018.
(58) Zeng, M.; Wang, Y.; Liu, Q.; Yuan, X.; Zuo, S.; Feng, R.; Yang, J.; Wang, B.; Qi, C.; Lin, Y. Encaging palladium nanoparticles in chitosan modified montmorillonite for efficient, recyclable catalysts. *ACS applied materials & interfaces* **2016,** *8* (48), 33157-33164.
(59) Bhawani, S. A.; Tariq, A.; Moheman, A.; Ngaini, Z. Chapter 5 - Functionalized Graphene Nanocomposites for Water Treatment. In *Functionalized Graphene Nanocomposites and their Derivatives*; Jawaid, M.; Bouhfid, R.; Kacem Qaiss, A. e., Eds.; Elsevier: 2019; pp 91-107.
(60) Fu, L.; Lai, G.; Zhu, D.; Jia, B.; Malherbe, F.; Yu, A. Advanced Catalytic and Electrocatalytic Performances of Polydopamine-Functionalized Reduced Graphene Oxide-Palladium Nanocomposites. *ChemCatChem* **2016,** *8* (18), 2975-2980.
(61) Fan, L.; Luo, C.; Li, X.; Lu, F.; Qiu, H.; Sun, M. Fabrication of novel magnetic chitosan grafted with graphene oxide to enhance adsorption properties for methyl blue. *Journal of Hazardous Materials* **2012,** *215-216*, 272-279.
(62) Ciganda, R.; Li, N.; Deraedt, C.; Gatard, S.; Zhao, P.; Salmon, L.; Hernández, R.; Ruiz, J.; Astruc, D. Gold nanoparticles as electron reservoir redox catalysts for 4-nitrophenol reduction: a strong stereoelectronic ligand influence. *Chemical Communications* **2014,** *50* (70), 10126-10129.
(63) Nejad, M. S.; Seyedi, N.; Sheibani, H. Fabrication of functionalized two dimensional graphene oxide and promoted with phosphotungstic acid for reduction of organic dyes in water. *Materials Chemistry and Physics* **2019,** *238*, 121849.
(64) Ncube, P.; Bingwa, N.; Baloyi, H.; Meijboom, R. Catalytic activity of palladium and gold dendrimer-encapsulated nanoparticles for methylene blue reduction: a kinetic analysis. *Applied Catalysis A: General* **2015,** *495*, 63-71.
(65) Wu, T.; Ma, J.; Wang, X.; Liu, Y.; Xu, H.; Gao, J.; Wang, W.; Liu, Y.; Yan, J. Graphene oxide supported Au–Ag alloy nanoparticles with different shapes and their high catalytic activities. *Nanotechnology* **2013,** *24* (12), 125301.
(66) Xu, L.; Wu, X.-C.; Zhu, J.-J. Green preparation and catalytic application of Pd nanoparticles. *Nanotechnology* **2008,** *19* (30), 305603.
(67) Hemmati, S.; Mehrazin, L.; Ghorban, H.; Garakani, S. H.; Mobaraki, T. H.; Mohammadi, P.; Veisi, H. Green synthesis of Pd nanoparticles supported on reduced graphene oxide, using the extract of Rosa

canina fruit, and their use as recyclable and heterogeneous nanocatalysts for the degradation of dye pollutants in water. *RSC advances* **2018,** *8* (37), 21020-21028.
(68) Navalon, S.; Dhakshinamoorthy, A.; Alvaro, M.; Garcia, H. Metal nanoparticles supported on two-dimensional graphenes as heterogeneous catalysts. *Coordination Chemistry Reviews* **2016,** *312*, 99-148.
(69) Ilunga, A. K.; Khoza, T.; Tjabadi, E.; Meijboom, R. Effective Catalytic Reduction of Methyl Orange Catalyzed by the Encapsulated Random Alloy Palladium-Gold Nanoparticles Dendrimer. *ChemistrySelect* **2017,** *2* (30), 9803-9809.
(70) Omidvar, A.; Jaleh, B.; Nasrollahzadeh, M. Preparation of the GO/Pd nanocomposite and its application for the degradation of organic dyes in water. *Journal of colloid and interface science* **2017,** *496*, 44-50.
(71) Hatamifard, A.; Nasrollahzadeh, M.; Lipkowski, J. Green synthesis of a natrolite zeolite/palladium nanocomposite and its application as a reusable catalyst for the reduction of organic dyes in a very short time. *RSC Advances* **2015,** *5* (111), 91372-91381.
(72) Fu, G.; Tao, L.; Zhang, M.; Chen, Y.; Tang, Y.; Lin, J.; Lu, T. One-pot, water-based and high-yield synthesis of tetrahedral palladium nanocrystal decorated graphene. *Nanoscale* **2013,** *5* (17), 8007-8014.
(73) Wang, F.; Shao, M.; Cheng, L.; Chen, D.; Fu, Y.; Ma, D. D. D. Si/Pd nanostructure with high catalytic activity in degradation of eosin Y. *Materials Research Bulletin* **2009,** *44* (1), 126-129.
(74) Sivaranjan, K.; Vanitha, P.; Sathiyaseelan, A.; Kalaichelvan, P.; Sathuvan, M.; Rengasamy, R.; Santhanalakshmi, J. Insights into the catalytic reduction of organic dyes and antibacterial activity of graphene oxide supported mono and bimetallic nanocomposites. *New Journal of Chemistry* **2017,** *41* (11), 4348-4359.